

Photocatalytic application of nanosized CdS immobilized onto functionalized MWCNTs

Cite this: *Dalton Trans.*, 2014, **43**, 7429

D. D. Chronopoulos,^a N. Karousis,^a S. Zhao,^b Q. Wang,^b H. Shinohara^b and N. Tagmatarchis^{*a,b}

Nanosized semiconductor CdS immobilized onto modified multi-walled carbon nanotubes (MWCNTs) carrying poly(amidoamine) dendron units were visualized by HR-TEM. Evidently, spherical CdS nanoparticles 3–5 nm in diameter were identified. Moreover, EDX spectroscopy gave additional spectroscopic proof of the presence of CdS in the CdS-MWCNTs hybrid material. The photocatalytic activity of CdS-MWCNTs toward the decomposition of rhodamine B (RhB) was examined by monitoring spectral changes in the characteristic absorption band of RhB centred at 554 nm. The latter absorption band of RhB was found to continuously depress during visible light irradiation in the presence of CdS-MWCNTs, with faster kinetic rates as compared with the case when only reference CdS was present. The current result was rationalized in terms of efficient photoinduced electron-transfer from CdS to MWCNTs within the intrahybrid CdS-MWCNTs. In this frame, the suggested mechanism for the high and fast photocatalytic decomposition of RhB supports the accumulation of electrons in MWCNTs, which then react with molecular oxygen, thus reducing it to superoxide radical anion $O_2^{\cdot-}$ responsible for the generation of the highly reactive species of HO^{\cdot} and HOO^{\cdot} . The latter together with the holes generated in photo-excited CdS were responsible for the decomposition of RhB. Finally, the photocatalyst CdS-MWCNTs was recovered and efficiently reused for four consecutive catalytic cycles, thus highlighting its wider applicability in removing organic pollutants from water.

Received 27th November 2013,
Accepted 23rd December 2013

DOI: 10.1039/c3dt53338g

www.rsc.org/dalton

Introduction

In recent years, there is great risk to human health and ecological systems from the release of synthetic pigments, dyes and pollutants in the environment.¹ Therefore, it is absolutely necessary to effectively remove such hazardous organic dyes from the atmosphere and in particular from wastewater. Along these lines, photocatalysis is a promising technology for decomposition of noxious waste by oxidative reactive species.² The latter can be generated by molecular oxygen in the presence of accumulated electrons (*i.e.* by reduction of O_2), those for example that are yielded in donor-acceptor ensembles upon electron-transfer phenomena at the acceptor site.

For such reasons, semiconductor nanoparticles attracted increased interest during the last decade,^{3,4} especially due to the advantageous function of inorganic quantum dots in capturing incident photons to induce charge separation.⁵ In particular, TiO_2 , although being among the most examined,

cheap and chemically stable semiconductors, suffers from poor absorption in an extended window of the solar spectrum,⁶ and thus it is photocatalytically active for the degradation of environmental pollutants only under UV irradiation.⁷ Therefore, other semiconductor materials with increased solar energy conversion efficiency and a slow recombination rate of the photogenerated electrons and holes are sought.⁸ In this context, visible light can be more competently harvested by CdS nanoparticles due to their narrow bandgap. In addition, integration of CdS to carbon nanotubes (CNTs) gives rise to novel electron donor-acceptor hybrid nanostructures in which intrahybrid electron-transfer events can lead to spatial separation of the photoinduced generated electrons and holes,⁹ thus decelerating the recombination rate and resulting in an increase of the corresponding lifetime and photocatalytic efficiency.

Recently, a few ensembles in which the CdS were integrated into CNTs, either *via* covalent or supramolecular means,^{9,10} mainly aiming to tackle energy conversion issues, have been reported. However, to the best of our knowledge, the photocatalytic application of covalently functionalized CdS-CNT hybrids in removing organic dyes from water yet awaits exploration. Even hybrid systems in which the CdS was integrated into CNTs *via* supramolecular means or in composite forms, with the inherent handicap of weaker interactions

^aTheoretical and Physical Chemistry Institute, National Hellenic Research Foundation, 48 Vassileos Constantinou Avenue, Athens 11635, Greece.

E-mail: tagmatarchis@iee.gr; Fax: +30 210 7273794; Tel: +30 210 7273835

^bDepartment of Chemistry and Institute for Advanced Research, Nagoya University, Nagoya 464-8602, Japan

between the two species due to inefficient stable anchoring of the semiconductor nanoparticles to CNTs, were rarely explored as photocatalysts.¹¹

Having succeeded on higher loading of CdS onto covalently modified multi-walled carbon nanotubes (MWCNTs) carrying poly(amidoamine) (PAMAM) dendron units ending in an ethylenediamine core,¹² which served as a template for the stabilization of monodispersed CdS nanoparticles, our research efforts were directed on the examination of that CdS-MWCNTs hybrid material toward the photocatalytic degradation of rhodamine B (RhB). Herein, it is shown that the presence of CdS nanoparticles uniformly immobilized onto PAMAM-modified MWCNTs is able under visible illumination to induce decomposition of aqueous RhB, with fast kinetic rates, due to the electron-transfer processes that occur within the hybrid nanostructure.

Results and discussion

Preparation and characterization of CdS-MWCNTs

The preparation of CdS-MWCNTs material was accomplished following our recently reported method.¹² Briefly, amino-terminated aryl-functionalized MWCNTs were used as a scaffold for the step-by-step growth of a second-generation one-branched dendron, carrying four terminal carboxyl groups per aryl unit grafted onto the skeleton of MWCNTs. These carboxylic units acted as anchor sites for the stabilization of Cd²⁺ ions, which were subsequently converted to CdS nanoparticles after mild thermal treatment with thiourea to yield CdS-MWCNTs (Chart 1). The detailed spectroscopic characterization of CdS-MWCNTs has already been reported, while fluorescence emission studies showed that upon photoillumination of CdS-MWCNTs the characteristic strong and broad emission of CdS nanoparticles was quantitatively quenched by the presence of MWCNTs.¹² The latter was indicative of strong

electronic interactions between CdS and MWCNTs and furthermore suggested electron and/or energy transfer processes from CdS to MWCNTs within the hybrid material,¹² similar to cases of other hybrid materials composed of CdS and CNTs.¹³

Focusing on the morphology, shape and size of CdS-MWCNTs, HR-TEM imaging revealed the immobilization of nanosized spherical CdS onto the PAMAM-modified MWCNTs. Actually, HR-TEM imaging of CdS-MWCNTs under low-magnification conditions showed high density coverage of the MWCNTs with CdS of around 15 nm in diameter (Fig. 1a). However, detailed analysis under high-magnification conditions illustrated that clustering of smaller-sized CdS nanoparticles (*i.e.* around 3–5 nm in diameter) occurs (Fig. 1b). Furthermore, direct proof that the aforementioned spherical nanoparticles are due to immobilized CdS arose from energy dispersive X-ray (EDX) spectroscopy, since the latter is a widely applied surface technique to study the elemental composition of nanostructured carbon-based hybrid materials. Thus, in the EDX spectrum of CdS-MWCNTs the presence of both cadmium and sulfur in the hybrid material was verified, yet with a 1 : 1 average atom ratio of Cd/S over the selected area (Fig. 1c).

For comparison purposes and to be used as reference material for the photocatalytic degradation of RhB (see below), CdS nanoparticles were synthesized in the absence of MWCNTs. In this frame, following similar experimental procedures like for the case of CdS-MWCNTs, reference CdS nanoparticles were stabilized upon treatment with 6-(BOC-amino)caproic acid. Likewise with the CdS-MWCNTs hybrid material, HR-TEM imaging revealed the success of the reference CdS formation, by observing aggregated spherical nanoparticles with an average diameter of 50–70 nm (Fig. 1d), consisting of smaller CdS nanoparticles of 5 nm in diameter (Fig. 1e). EDX spectroscopy of reference CdS further proved their efficient formation by observing the characteristic peaks for cadmium and sulphur (Fig. 1f).

Photocatalytic degradation of RhB

The photocatalytic activity of nanosized CdS immobilized on the PAMAM-functionalized MWCNTs was examined by monitoring the degradation of RhB under visible light irradiation. In this frame, temporal changes in the concentration of RhB were checked by inspecting variations occurring at the characteristic absorption band of RhB centered at 554 nm. Initially, it was confirmed that the absorption band of an aqueous solution of RhB (*i.e.* 554 nm) remained unchanged even after 3 h of visible light irradiation. Then, for the current study, in an aqueous solution of RhB (5 mL, 10⁻⁵ M), 5 mg of CdS-MWCNTs (*i.e.* CdS loading: 0.14 μmol mg⁻¹ as calculated by thermogravimetry) as a photocatalyst was added and the system was stirred in the dark for 30 min in order to establish a suitable adsorption–desorption equilibrium between RhB and the catalyst surface. UV-Vis spectroscopy (Fig. 2a) indicated that the main band of RhB at 554 nm was practically flattened after *ca.* 60 min of visible light irradiation in the presence of air, thus suggesting the complete photocatalytic degradation of RhB by the presence of CdS-MWCNTs. It is

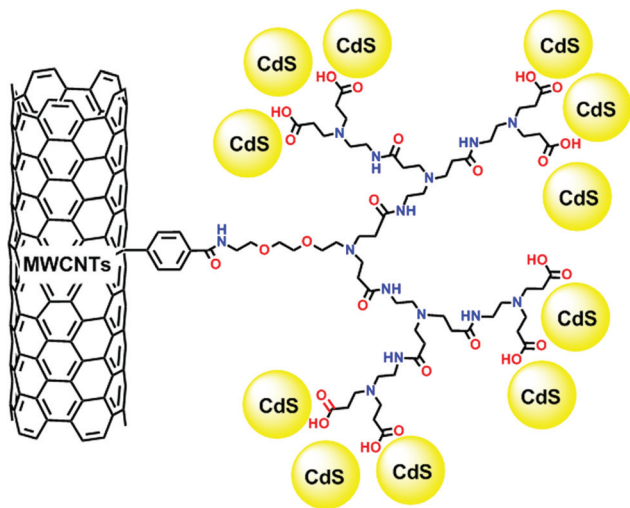


Chart 1 Partial structure of nanosized CdS immobilized onto PAMAM-modified MWCNTs.

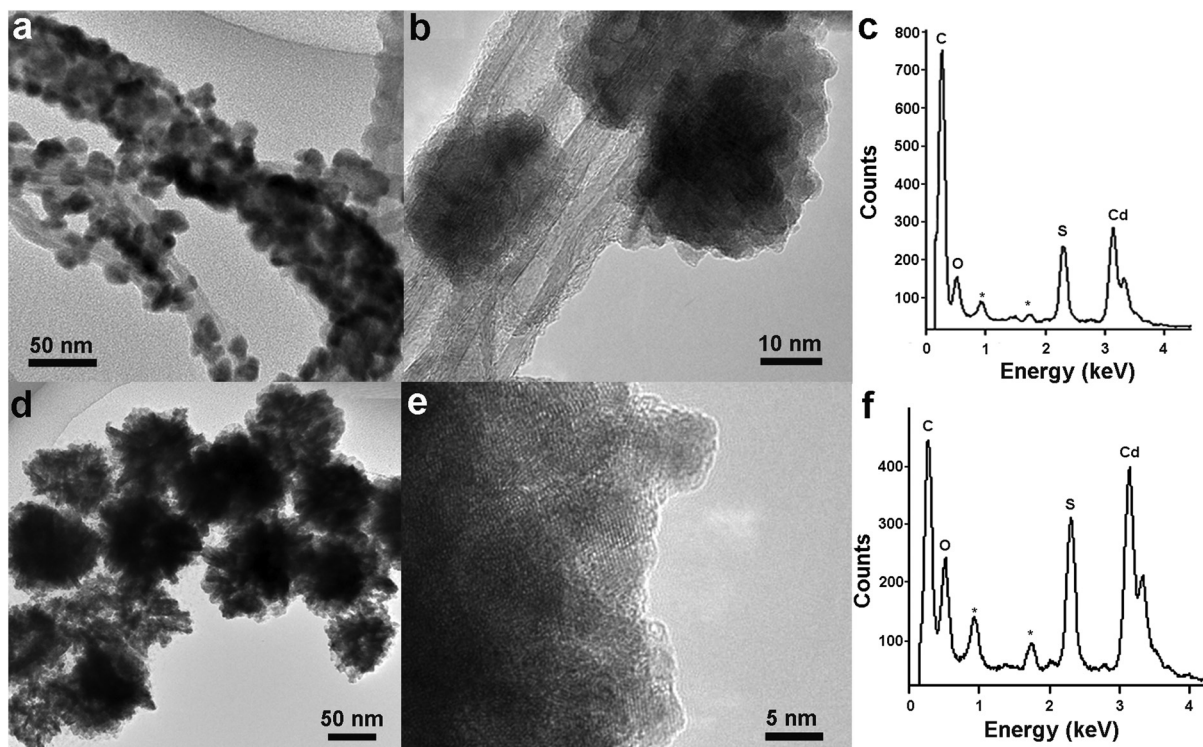


Fig. 1 Low (a, d) and high (b, e) magnification HR-TEM images and EDX spectra (c, f) of CdS-MWCNTs hybrid material and reference CdS respectively. In the EDX spectra (c, f), stars denote the elements Cu and Si which are detected because of their presence in the microscope equipment, sample holder, and crystal detector.

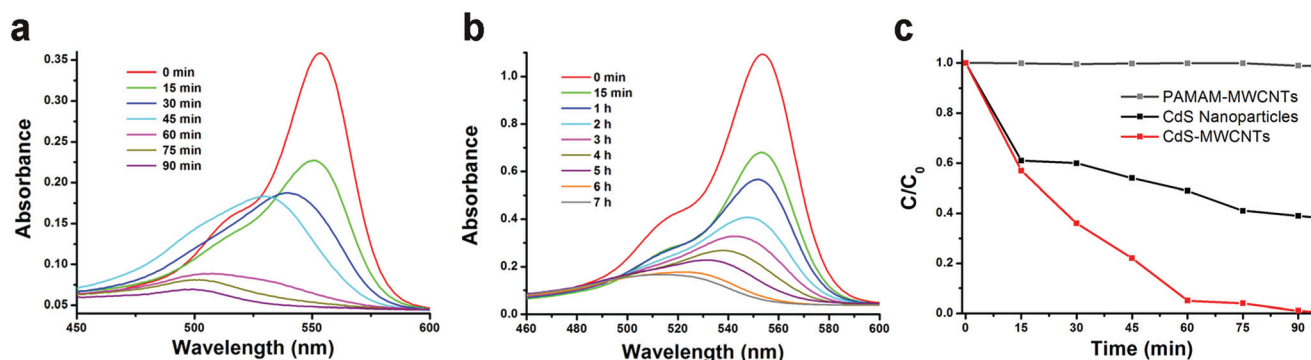


Fig. 2 UV-Vis spectral changes of aqueous RhB in the presence of (a) CdS-MWCNTs hybrid material, and (b) reference CdS, under visible light irradiation in the presence of air. (c) Photocatalytic performance of CdS-MWCNTs (red), reference CdS (black) and reference PAMAM-modified MWCNTs (grey) in the degradation of aqueous RhB under visible light irradiation in the presence of air.

noteworthy that continuous and significant quenching of the maximum absorbance of RhB took place during visible light irradiation in the presence of CdS-MWCNTs, thus highlighting the degradation of the xanthen conjugated system in RhB.¹⁴ At the same time, the maximum of the main absorption band of RhB was gradually blue-shifted by 56 nm (*i.e.* from 554 to 498 nm) and completed within 90 min of photoirradiation, thus supporting the complete *N*-de-ethylation of RhB to rhodamine.¹⁵ Actually, careful inspection on the temporal changes occurred in the absorption spectrum of photoirradiated RhB in the presence of CdS-MWCNTs as the photocatalyst revealed the

stepwise *N*-de-ethylation of RhB; namely, one and three ethyl groups were lost after 30 and 60 min of light irradiation, respectively.¹⁶ The latter is justified by monitoring the formation of new absorption bands at 539 nm and 508 nm due to the formation of *N,N,N'*-triethyl rhodamine and *N*-ethyl rhodamine, respectively, before accessing the fully *N*-de-ethylated rhodamine (Chart 2) with characteristic absorption centered at 498 nm.¹⁵ At this stage it should also be mentioned that without visible light irradiation but in the presence of CdS-MWCNTs, the absorption profile of RhB remained unaltered, thus highlighting the necessity of light for the decomposition process.

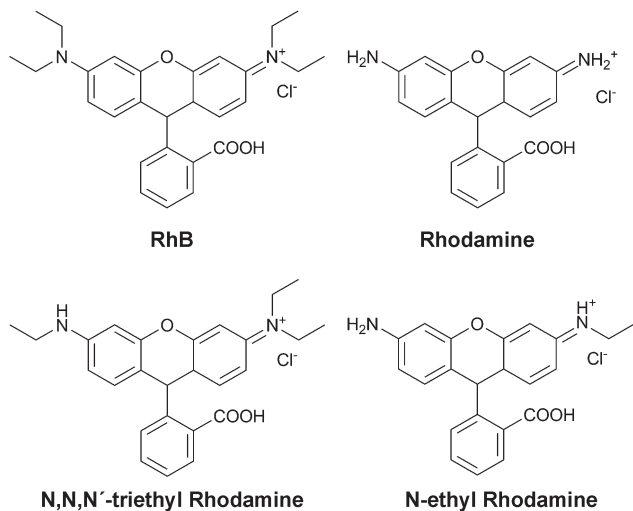


Chart 2 Molecular structures of RhB and the *N*-de-ethylated byproducts rhodamine, *N,N,N'*-triethyl rhodamine and *N*-ethyl rhodamine formed during visible light photodegradation of RhB by CdS-MWCNTs in the presence of air.

Control experiments performed in order to test if the photocatalytic degradation of RhB proceeds – and to what extent, if it occurs – in the presence of PAMAM-modified MWCNTs (*i.e.* without CdS) and in the presence of reference CdS nanoparticles (*i.e.* without MWCNTs). Evidently, while upon visible light irradiation, photodegradation of RhB in the presence of PAMAM-modified MWCNTs was negligible (if not at all), reference CdS nanoparticles showed moderate photocatalytic activity (*i.e.* the UV-Vis spectral changes of RhB in the presence of reference CdS are displayed in Fig. 2b), however, with rather slower kinetics as compared with the ones observed for the CdS-MWCNTs hybrid material (*cf.* Fig. 2a). Thus, as the graph for the temporal course of the photodegradation of RhB shows (Fig. 2c), in 60 min only 50% of RhB was photodecomposed by the reference CdS, while after the same elapsed period more than 95% of RhB was degraded by CdS-MWCNTs. In addition, control experiments in the absence of air were negative, thus suggesting the necessity of the latter as discussed in the mechanism of photodegradation of RhB below.

Recovery and reuse of CdS-MWCNTs for the photocatalytic degradation of RhB

In order to evaluate the photocatalytic stability of CdS-MWCNTs hybrid material, the recyclability of the catalyst in the photodegradation of RhB under visible light irradiation was tested. In this context, CdS-MWCNTs were recovered after completion of the first run by filtration, then washed with water to remove any organic material entrapped and then reused by adding it to a freshly prepared aqueous solution of RhB of the same concentration as the initial one (*i.e.* 5 mL, 10^{-5} M). Four successive catalytic cycles were performed and all degradation efficiencies toward RhB obtained after 90 min of visible irradiation were slightly compromised but always found above 90% as compared with the first run. Based on

these results the number of turnovers (TON), namely the number of substrate molecules that a molecule of catalyst can convert to products under a certain set of experimental conditions, was calculated and found to be 14. At the same time, the turnover frequency (TOF) for the same set of experiments remained unchanged and found to be 9.5 h^{-1} . To the best of our knowledge, these TON and TOF values are the highest obtained, although yet not optimized, for evaluating the efficiency of recovery and reuse of CdS-MWCNTs for the photocatalytic degradation of RhB.

Mechanism for the photocatalytic degradation of RhB by CdS-MWCNTs

The enhancement of the photocatalytic degradation of RhB by CdS-MWCNTs as opposed to reference CdS is rationalized in terms of the effective separation of holes–electrons in photo-excited CdS. This is to say that electron-transfer from photo-excited CdS to MWCNTs, within CdS-MWCNTs hybrid, occurs.⁹ Then, the electrons accumulated in MWCNTs react with molecular oxygen, thus reducing it to superoxide radical anion $\text{O}_2^{\cdot-}$ responsible for the generation of the highly reactive species of HO^{\cdot} and HOO^{\cdot} . Eventually, degradation of RhB occurs by the holes generated in CdS and the powerful oxidizing species of HO^{\cdot} and HOO^{\cdot} capable of degrading most pollutants.¹⁷ Based on the aforementioned mechanism, it is understandable that charge separation in CdS-MWCNTs is the process that governs the photodecomposition of RhB as opposed to the case of reference CdS, since in the latter a rapid recombination of the hole–electron pair is inevitable due to the absence of suitable electron acceptor units such as MWCNTs are. The photocatalytic mechanism for the action of CdS-MWCNTs in the decomposition of RhB is schematically illustrated in Fig. 3.

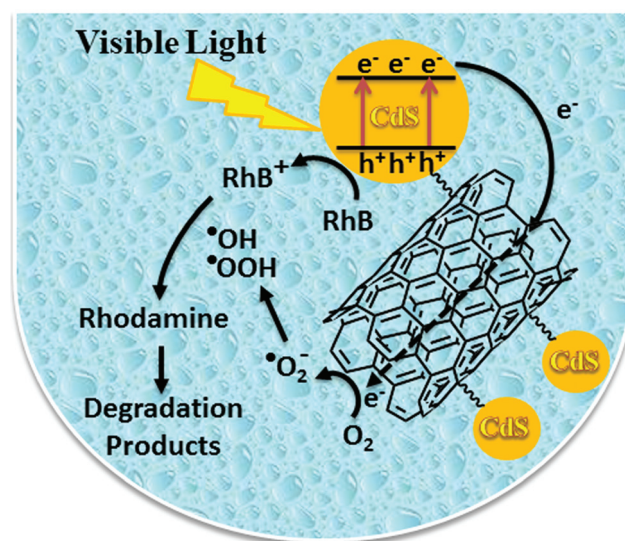


Fig. 3 Schematic illustration for the electron-transfer process within CdS-MWCNTs responsible for the photocatalytic degradation of aqueous RhB under visible light irradiation in the presence of air.

Conclusions

Summarizing, the application of CdS-MWCNTs on the photo-degradation of RhB upon visible light irradiation in the presence of air was successful. Initially, the immobilized CdS nanoparticles on PAMAM-modified MWCNTs were monitored by extensive HR-TEM imaging, highlighting the presence of CdS as round objects with a diameter of 3–5 nm, which were further spectroscopically identified by EDX analysis. Then, the high visible-light photocatalytic performance of CdS-MWCNTs toward decomposition of RhB was demonstrated by monitoring temporal changes in the concentration of RhB as followed by changes observed in the characteristic absorption band of RhB centered at 554 nm. The CdS-MWCNTs hybrid material was recovered simply by filtration, re-used and found to efficiently catalyze the degradation of RhB for four successive cycles. The high photocatalytic activity of CdS-MWCNTs was facilitated by the separation of the photogenerated electron-hole pair in CdS due to efficient photoinduced electron-transfer from CdS to MWCNTs and the accumulation of electrons in MWCNTs, which can then react with molecular oxygen, thus reducing it to superoxide radical anion $O_2^{\cdot-}$ responsible for the generation of the highly reactive species of HO^{\cdot} and HOO^{\cdot} . The latter together with the holes generated in photo-excited CdS were responsible for the degradation of RhB.

Experimental

General

All solvents and reagents were purchased from Aldrich and used without further purification unless otherwise stated. CdS-decorated PAMAM-modified MWCNTs and reference CdS were synthesized according to previously reported procedures.¹² Steady-state UV-Vis electronic absorption spectra were recorded on a Perkin Elmer (Lambda 19) UV-Vis-NIR spectrophotometer. HR-TEM measurements were carried out using a JEM-2100F (JEOL) high-resolution field-emission gun TEM operated at 80 keV at room temperature and under a pressure of 10^{-6} Pa. HR-TEM images were recorded with a charge-coupled device with an exposure time of typically 1 s. Energy dispersive X-ray (EDX) spectroscopy measurements were performed using the same microscope equipped with a super atmospheric thin-window X-ray detector.

Degradation of aqueous RhB

The degradation of aqueous RhB was carried out in a special Pyrex vessel which was positioned inside a cylindrical vessel surrounded by a circulating aqueous solution $NaNO_2$ 1 M as a UV-cut-off filter, thus ensuring that illumination was only by visible light. The light source used was a 500 W xenon lamp, which was positioned 20 cm away from the reactor. The photocatalyst (5 mg, $0.14 \mu\text{mol mg}^{-1}$) was added into the aqueous solution of RhB (5 mL, 10^{-5} M) with full stirring in the dark for about 30 min in order to achieve a suitable adsorption-desorption equilibrium of the dye on the surface of the catalyst.

At given irradiation time intervals, 3 mL of the reaction mixture was sampled and separated by centrifugation. The concentration of RhB was determined by monitoring changes in the absorption band centered at 554 nm.

Acknowledgements

Partial financial support by the Japan Society for the Promotion of Science (JSPS) Program "FY2012 JSPS Invitation Fellowship for Research in Japan – Long Term" contract number L-12531 to NT is acknowledged.

Notes and references

- 1 E. Forgacs, T. Cserhati and G. Oros, *Environ. Int.*, 2004, **30**, 953–971.
- 2 (a) L. Ge, M. X. Xu and H. B. Fang, *J. Mol. Catal. A: Chem.*, 2006, **256**, 68–76; (b) Z. Y. Zhang, F. Zuo and P. Y. Feng, *J. Mater. Chem.*, 2010, **20**, 2206–2212; (c) Y. L. Lai, M. Meng, Y. F. Yu, X. T. Wang and T. Ding, *Appl. Catal., B*, 2011, **105**, 335–345.
- 3 A. G. Pattantyus-Abraham, I. J. Kramer, A. R. Barkhouse, X. H. Wang, G. Konstantatos, R. Debnath, L. Levina, I. Raabe, M. K. Nazeeruddin, M. Graetzel and E. H. Sargent, *ACS Nano*, 2010, **4**, 3374–3380.
- 4 (a) U. I. Gaya and A. H. Abdullah, *J. Photochem. Photobiol., C*, 2008, **9**, 1–12; (b) C. S. Guo, M. Ge, L. Liu, G. D. Gao, Y. C. Feng and Y. Q. Wang, *Environ. Sci. Technol.*, 2010, **44**, 419–425.
- 5 (a) M. G. Walter, E. L. Warren, J. R. McKone, S. W. Boettcher, Q. Mi, E. A. Santori and N. S. Lewis, *Chem. Rev.*, 2010, **110**, 6446–6473; (b) K. Maeda and K. Domen, *J. Phys. Chem. Lett.*, 2010, **1**, 2655–2661; (c) P. V. Kamat, *J. Phys. Chem. Lett.*, 2012, **3**, 663–672.
- 6 (a) R. Asahi, T. Morikawa, T. Ohwaki, K. Aoki and Y. Taga, *Science*, 2001, **293**, 269–271; (b) L. Ge, M. Xu, H. Fang and M. Su, *Appl. Surf. Sci.*, 2006, **253**, 720–725.
- 7 (a) J. M. Szeifert, J. M. Feckl, D. Fattakhova-Rohlfing, Y. J. Liu, V. Kalousek, J. Rathousky and T. Bein, *J. Am. Chem. Soc.*, 2010, **132**, 12605–12611; (b) K. Park, Q. F. Zhang, B. B. Garcia, X. Y. Zhou, Y. H. Jeong and G. Z. Cao, *Adv. Mater.*, 2010, **22**, 2329–2332; (c) Y. Jin, G. Zhao, M. Wu, Y. Lei, M. Li and X. Jin, *J. Phys. Chem. C*, 2011, **115**, 9917–9925.
- 8 (a) J. Ren, W. Z. Wang and S. M. Sun, *Appl. Catal., B*, 2009, **92**, 50–55; (b) M. C. Long, W. M. Cai, J. Cai, B. X. Zhou, X. Y. Chai and Y. H. Wu, *J. Phys. Chem. B*, 2006, **110**, 20211–20216.
- 9 (a) I. Robel, B. A. Bunker and P. V. Kamat, *Adv. Mater.*, 2005, **17**, 2458–2463; (b) G. Mountrichas, S. Pispas and N. Tagmatarchis, *Small*, 2007, **3**, 404–407; (c) G. Mountrichas, A. S. D. Sandanayaka, S. P. Economopoulos, S. Pispas, O. Ito, T. Hasobe and N. Tagmatarchis, *J. Mater. Chem.*, 2009, **19**, 8990–8998;

- (d) X. L. Li, Y. Jia, J. Q. Wei, H. W. Zhu, K. L. Wang, D. H. Wu and A. Y. Cao, *ACS Nano*, 2010, **4**, 2142–2148.
- 10 (a) J. Shi, Y. Qin, W. Wu, X. Li, Z.-X. Guo and D. Zhu, *Carbon*, 2004, **42**, 455–458; (b) L. Sheeney-Haj-Ichia, B. Basnar and I. Willner, *Angew. Chem., Int. Ed.*, 2005, **44**, 78–83; (c) R. Loscutova and A. R. Barron, *J. Mater. Chem.*, 2005, **15**, 4346–4353; (d) C. Li, Y. Tang, K. Yao, F. Zhou, Q. Ma, H. Lin, M. Tao and J. Liang, *Carbon*, 2006, **44**, 2021–2026; (e) G. M. Neelgund, A. Oki and Z. Luo, *Colloids Surf., B*, 2012, **100**, 215–221; (f) P. Baviskar, P. Chavan, N. Kalyankar and B. Sankapal, *Appl. Surf. Sci.*, 2012, **258**, 7536–7539.
- 11 (a) G. M. Neelgund and A. Oki, *Appl. Catal., B*, 2011, **110**, 99–107; (b) H. Li, X. Gui, C. Ji, P. Li, Z. Li, L. Zhang, E. Shi, K. Zhu, J. Wei, K. Wang, H. Zhu, D. Wu and A. Cao, *Nano Res.*, 2012, **5**, 265–271; (c) A. Ye, W. Fan, Q. Zhang, W. Deng and Y. Wang, *Catal. Sci. Technol.*, 2012, **2**, 969–978; (d) X. Wang, M. Liu, Q. Chen, K. Zhang, J. Chen, M. Wang, P. Guo and L. Guo, *Int. J. Hydrogen Energy*, 2013, **38**, 13091–13096; (e) H.-Y. Zhu, G. Yao, R. Jiang, Y.-Q. Fu, Y.-H. Wu and G.-M. Zeng, *Ceram. Int.*, 2014, **40**, 3769–3777.
- 12 D. Chronopoulos, N. Karousis and N. Tagmatarchis, *ECS J. Solid State Sci. Technol.*, 2013, **2**, M3023–M3027.
- 13 S.-H. Hwang, C. N. Moorefield, P. Wang, K.-U. Jeong, S. Z. D. Cheng, K. K. Kotta and G. R. Newkome, *J. Am. Chem. Soc.*, 2006, **128**, 7505–7509.
- 14 C. C. Chen, W. Zhao, P. X. Lei, J. C. Zhao and S. Nick, *Chem.–Eur. J.*, 2004, **10**, 1956–1965.
- 15 T. Watanabe, T. Takizawa and K. Honda, *J. Phys. Chem.*, 1977, **81**, 1845–1851.
- 16 The formation of the photodegraded byproduct of RhB having lost two ethyl units was not observed in the evolved UV-Vis spectra; however, it is expected that it was formed after 30–60 min of visible light irradiation.
- 17 M. R. Hoffmann, S. T. Martin, W. Choi and D. W. Bahnemann, *Chem. Rev.*, 1995, **95**, 69–96.